ETH *zürich*

Compact MR-compatible DC-DC converter module

Journal Article

Author(s):
Ritzer, Christian; Commichau, Volker; Dhawan, Satish K.; Fischer, Jannis (iD); Lustermann, Werner; Sumner, Robert; Warnock, Geoffrey; Dissertori, Günther

SISSA

Compact MR-compatible DC-DC converter module

View the article online for updates and enhancements.

IOP ebooks™

Bringing you innovative digital publishing with leading voices to create your essential collection of books in STEM research.

Start exploring the collection - download the first chapter of every title for free.

Compact MR-compatible DC-DC converter module

C. Ritzer,[a,1] **V. Commichau,**[a] **S.K. Dhawan,**[b] **J. Fischer,**[a] **W. Lustermann,**[a] **R. Sumner,**[c] **G. Warnock**[d] **and G. Dissertori**[a]

[a] *Institute for Particle Physics and Astrophysics, ETH Zürich,*
 Otto-Stern-Weg 5, Zürich, Switzerland

[b] *Department of Physics, Yale University, 217 Prospect Street, New Haven, U.S.A.*

[c] *Cheesecote Mountain Consultants, 24 Halley Drive, Ponoma, U.S.A.*

[d] *Institute for Pharmacology and Toxicology, University of Zürich,*
 Winterthurerstrasse 190, Zürich, Switzerland

 E-mail: critzer@phys.ethz.ch

ABSTRACT: The SAFIR collaboration is developing a high rate positron emission tomography insert for a preclinical 7 T magnetic resonance imaging (MRI) device. To meet the desired performance figures, a large number of readout channels (≈ 15000) and integration of data digitisation into the insert are required. Consequently, the insert will consume about 1.3 kW of input power at low voltages (≤ 3.3 V). This corresponds to large supply currents of several 100 A, requiring heavy and bulky supply cables. To overcome these problems we developed a compact and MR-compatible DC-DC stepdown converter module. Our converter is based on an air core inductor and is optimised for low electromagnetic emissions. It has an input voltage range from 6 V to 24 V and provides an adjustable output voltage from 1 V almost up to the input voltage. The maximum continuous output current is 6 A.

We measured conversion efficiencies between 70 % and 87% depending on output load and input voltage. For the operation conditions foreseen (16 V input voltage, 2.4 V output voltage and 3 A output current), we achieved an efficiency of 83.8%. Our tests inside the MRI demonstrated the compatibility between the MRI system and the step-down converters developed. No mutual interference was observed. The signal-to-noise ratio of the MRI remains unaltered, independent of the activity of the step-down converter under any operation condition and no effect on the operation of the DC-DC converter was observed.

This successful test of an MR-compatible DC-DC converter creates new opportunities for the power supply of complex hardware inside an MRI. 49 of the DC-DC converters will be used in our SAFIR PET insert, but they can also be used in other applications with high power demand in environments with strong magnetic fields.

---

[1]Corresponding author.

Contents

1 Introduction

The SAFIR collaboration was formed to develop a positron emission tomography (PET) insert, which is compatible with an existing preclinical magnetic resonance imaging (MRI) system (Bruker BioSpec 70/30) [1, 2]. In contrast to other PET inserts, an important part of the SAFIR specification is continued accurate function at high count rates (high radioactivity in field-of-view), providing good count statistics for very short time frames (< 5 s). [3–5] The superconducting magnet of the MRI creates a static 7 T B_0-field. Its gradient system (B-GA 20S) has a maximum gradient strength

of 0.2 T/m and a maximum slew rate of 640 T/sm. The inner diameter is 200 mm, which limits the outer diameter of the insert. Furthermore the foreseen MRI RF coils (suitable for rat whole body imaging) have an outer diameter of 114 mm. The remaining ring of 43 mm width can be used for our electronics and mechanics.

The full detector will comprise 24 identical readout boards for data acquisition. Each supports 20 Application Specific Integrated Circuits (ASICs) for analogue signal handling, a Field Programmable Gate Array (FPGA) for digital signal processing, as well as an optical Ethernet link for communication and various buffer chips for fast signal distribution. The estimated power consumption per board (including losses in the power converters) is about 50 W. Seven intermediate rails (6x 2.4 V with $\approx$ 2.5 A and 1x 4.1 V with $\approx$ 2.0 A) are used to generate all voltages within these boards. In addition, there are several auxiliary boards, 24 for bias voltage generation and five for system clock distribution and timing synchronisation. We estimate a total power consumption of 1.3 kW, including losses in the used low drop-out regulators (LDOs), power converters and cabling. The main power supplies will be located outside the MRI room with a cable length of about 11 m. Three major problems are associated with supplying the required voltages directly. First, separate supply lines are needed for the different voltages. Second, the large currents require large wire cross sections in order to limit the voltage drop. Third, the limited space at the end of the PET insert is not sufficient to place the corresponding large connectors. Moreover, a remote sensing of the input voltage at the detector would be desirable to maintain a stable input voltage at different load conditions. This would further increase the number of connections. DC-DC converters placed inside the MRI bore solve all these problems. The input currents are lowered by a factor of five to six and the cabling is simplified, to a single input line with smaller wire cross section. In addition, remote sensing is not necessary in this configuration.

The MRI scanner's receive and transmit system operates at frequencies around 300 MHz, making it very susceptible to electromagnetic interference at this frequency. Commercially available DC-DC converters use ferromagnetic materials in the core, which are incompatible with operation in a 7 T field. Moreover, most designs have bad electromagnetic interference (EMI) characteristics. Until now, to the best of our knowledge, only one group ever suggested the usage of a commercial DC-DC module inside a 1.5 T MRI, but no results were published [6, 7].

In high energy physics, the usage of DC-DC converters was proposed but with slightly different requirements [8]. In these applications, radiation hardness is most important, such that commercial controller ASICs are excluded. This use case also involves strong magnetic fields (3.8 T in the compact muon solenoid [9]). We used this similarity as a starting point for our research. At CERN, there are so called FEASTMP modules available [10], which are radiation hard and magnetic field tolerant DC-DC converter modules (max. 12 V input, max. 10 W/4 A output). Such devices were successfully tested in the MRI. This inspired and encouraged our own development based on commercial controller ASICs, which would additionally allow for larger input voltages, larger load current and higher efficiency. For a successful test, we have to achieve an efficiency of at least 75 % without visible disturbances of the MRI images. The outcome of our efforts is presented in this work.

2 Materials

2.1 Schematic

Our development is based on the "LT8640S" ASIC from Analog Devices [11]. This device is a controller for step-down converters, specially designed for low radio frequency (RF) emission. In particular, all EMI critical bypass capacitors are integrated, reducing the dependence of the EMI performance from the printed circuit board (PCB) layout. Furthermore, the ASIC comes in a LQFN Package, which reduces trace lengths to the absolute minimum. It has a maximum input voltage of 42 V and a maximum continuous output current of 6 A. The schematic of our design is shown in figure 1. The input capacitors are rated for 25 V and thereby limit the maximum input voltage of
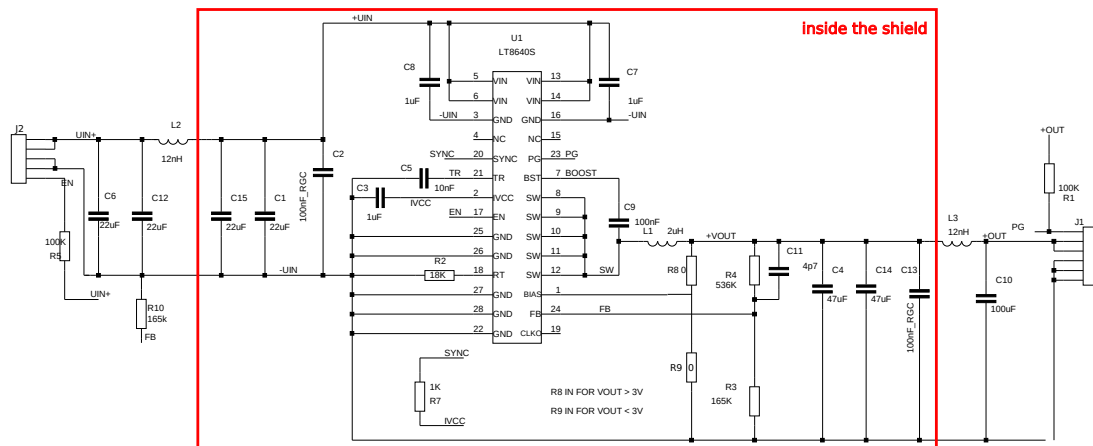
Figure 1. Schematic of the presented DC-DC converter module.

our converter module. The switching frequency is not fixed, but the minimum is set to 2 MHz (by resistor R2, figure 1) and the spectrum spread mode is activated. This feature of the controller ASIC modulates the switching frequency between 2.0 MHz and 2.4 MHz to prevent single emission peaks in the power spectrum. To reduce EMI emissions we added two reverse geometry capacitors (C2 and C13) close to the LT8640S ASIC. Moreover, there are low pass filters with a cut off frequency of ~ 200 kHz on the input and output of the converter module (L2 and L3). We use two standard pin headers (2.54 mm) for the electrical connections, with eleven pins in total. There are five ground lines, two input lines, two output lines, one enable line and a power good open collector line. The resistor R10 is placed outside of the shielding (figure 1), so that it can be changed easily. Together with R3 and R4 it defines the output voltage. We developed a second version of the converter, with one additional pin (twelve in total), so that the resistor R10 can be placed external to the converter module. For the measurements presented in this work, we selected 2.4 V as output voltage. In our final PET insert, this voltage is used to power 1.8 V LDOs for the components.

2.2 Design & layout

In general, the MRI scanner is sensitive to ferro magnetic materials (distortion of the B_0-field), eddy currents (distortion of the gradient pulses) and EMI (noise in the acquired signal). There are two current loops (input loop and output loop) in the DC-DC converter which cannot be avoided [12].

However we minimize the loop area to suppress EMI by placing the capacitors as close as possible to the ASIC. Furthermore, we deploy a two-part copper shield with a thickness of 0.2 mm around all main components (see schematics, figure 1). The two filters are placed outside of the shield to avoid coupling between the inductors. A via fence within the PCB closes the shield completely, with the exception of two inevitable gaps for input- and output-lines. Minimizing the area of the critical current loop is important for minimizing the radiated power. For that reason, a four layer PCB was chosen with an overall size of 17 mm × 33 mm. To ensure MR-compatibility, only non-magnetic materials can be used (eg. air coil inductors). A conventional ferro-magnetic core would distort the B_0-field and would always be saturated in the MRI. The two small coils in the filters are commercially available, while the main inductor is specially designed for this module. An image of the developed DC-DC converter is shown in figure 2.

Figure 2. A picture of the developed device, the main shield as well as the two filters on the in- and output are visible.

2.3 Main air-core inductor

We use a custom designed solenoid coil with an air core as main inductor. It has 16 windings of 0.8 mm enamelled copper wire (cross section 0.5 mm^2). The inductor is rectangular shaped and has outer dimensions of 4 mm × 8 mm × 13 mm. Due to the Lorentz force, it is necessary to soak the coil with glue (Araldite Rapid) and to attach it to the PCB. The final coil has an inductance of about 2.2 μH and a serial resistance of about 18 mΩ.

2.4 Emission measurement setup

The electromagnetic power radiated in the near field around 300 MHz is critical in our application. Measurements were done with a spectrum analyser (Rohde & Schwarz: FSH4) in combination with a near field probe (Langer EMV: RF-R 400-1). For the first measurement, the probe was placed 5 mm above the shield of our converter module. In addition we measured 5 mm below the bottom shield.

2.5 MRI measurement

We performed the MRI measurements inside a Bruker BioSpec 70/30 device with a Bruker B-GA 20S gradient system. The same power supply (Keysight E3645A) and the same electronics load (Mayuno DC Electronics load DC9711) were used, but they are placed outside of the Faraday cage. An eight-core cable with shielding connected the power converter in the scanner room with the power supply and load. The converter was placed centrally above the transmit- and receive coil

(Bruker "RF RES 300 1H 075/040 QNS TR"). We used an MR transparent plastic ring to fix the position of the power converter module 35 mm above the MR coil. A mouse sized phantom was placed centrally in the animal bed. The phantom had a volume of 50 mL and was filled with a standardized solution from Bruker (water with 1 g/L $CuSO_4$ and 3.6 g/L NaCl).

3 Methods

3.1 Static measurements

For the static measurements, we performed load-regulation and line-regulation tests. These were also used to evaluate the conversion efficiency. For all measurements we used a linear power supply (Keysight E3645A) and an electronics load (Mayuno DC Electronics load DC9712). We used 0.5 m of silicon cables with 0.5 mm^2 cross-section to connect the converter to the power supply as well as to the load. Sense wires on the input and the output were used to measure the voltages and to maintain a stable input voltage. We varied the load current between 0 A and 6 A in steps of 1 A. We used the voltages and currents to calculate the efficiency η, defined by:

$$\eta = \frac{P_{\text{out}}}{P_{\text{in}}},$$

with the output power P_{out} and the input power P_{in} of the converter module. Since the overall efficiency of the device is temperature dependent, it was switched off between the different measurement points, to avoid excessive heating. An external temperature sensor was attached to the copper shielding to verify that the device temperature was below 30 °C during each measurement. The maximum observed temperature increase was 3 K. Furthermore, we measured the output voltage and efficiency for a high load operation scenario (16 V input voltage and 4 A output current) at different device temperatures.

3.2 Dynamic measurements

In addition to the static measurements, we measured the transient behaviour of our power converter module. We applied load changes up to 6 A for a fixed input voltage of 16 V. We monitored the output voltage with an oscilloscope (LeCroy WaveRunner 640), directly at the output of the converter. The maximum voltage drop/overshoot together with the recovery time are reported.

3.3 Emission spectrum measurements

For the emission measurements, the converter was powered with 16 V by a linear power supply (Keysight E3645A). A constant load of 4 A was applied during the measurement (Mayuno DC Electronics load DC9712). The MRI is sensitive around 300 MHz and therefore we selected a measurement range from 297.5 MHz to 302.5 MHz. The resolution band width was set to 100 kHz and the video band width to 10 kHz. We used the built-in pre-amplifier of the spectrum analyser (gain x10). In addition, we measured the background spectrum and show it as comparison.

3.4 MRI measurements

Interference measurements in the MRI focused on distortions of the B_0-field and on parasitic coupling into the RF-system. The B_0-field was mapped within the water phantom with the standard

Bruker sequence (field of view: $40\,mm \times 40\,mm \times 40\,mm$; voxel size: $0.5\,mm \times 0.5\,mm \times 0.5\,mm$). The system was shimmed before each measurement and we present three slices of the B_0-map. To analyse the impact on the signal-to-noise ratio we used five repetitive measurements with the Bruker quality assurance sequence. This sequence is based on a T1-weighted sequence with automatic post-processing, which fits a circular region-of-interest to the phantom to obtain a signal region and four regions outside of that to get a background value. The signal-to-noise ratio is calculated and normalized to the image voxel volume. This test was performed without converter (a), with the converter module inside the MRI but not powered (b), powered with a load of 2 A (c) and powered with a load of 4 A (d).

4 Results

4.1 Static measurements

The results of our line- and load measurements are presented in figure 3. The output voltages dropped linearly by 70 mV with increasing load across the load range. The line regulation was much better and no deviation was observed. In addition we show the efficiency of the converter module at room temperature. The results are summarized in figure 4. The highest efficiency of
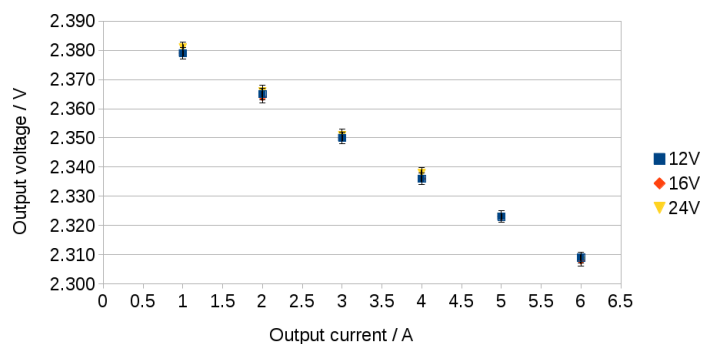
Figure 3. Load regulation measurements of our DC-DC converter module for three different input voltages (nominal output voltage 2.4 V at room temperature).
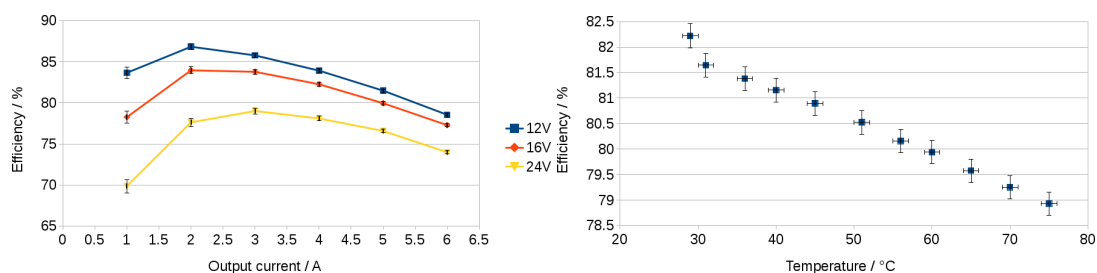
Figure 4. *Left:* measured efficiency of our DC-DC converter module at room temperature, *right:* and for higher temperatures with constant load (16 V input, 4 A load). The selected output voltage is 2.4 V.

86.8 % was measured at an input voltage of 12 V and with an output current of 2 A. For realistic operation conditions (16 V input voltage, 3 A load) the efficiency is 83.8 %. Finally we analysed the influence of different temperatures on the efficiency. The efficiency across the observed temperature range (30 °C to 75 °C) decreased by about 3 percent points down to 78.9 %. Efficiency decreased linearly with increasing temperature, with the exception of the first point.

4.2 Dynamic measurements

An example for the measured transient is shown in figure 5 for a fixed input voltage of 16 V and a load change from 0 A to 6 A. From this one can derive a maximum voltage drop of 350 mV. After
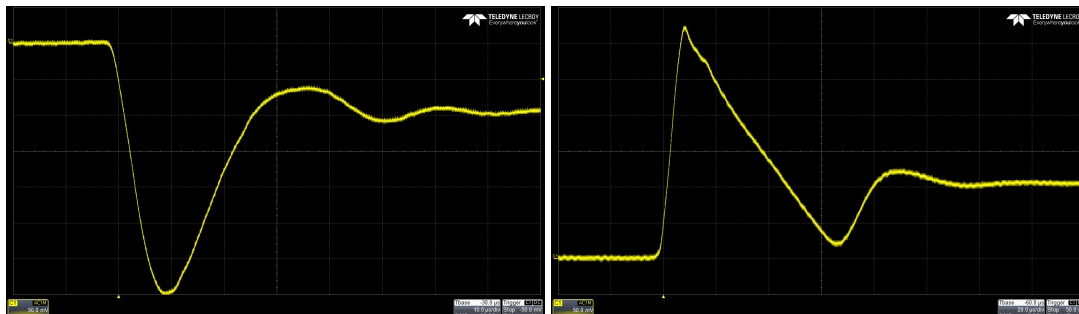
Figure 5. *Left:* measured transient for a load change from 0 A to 6 A, *right:* from 6 A to 0 A. The amplitude is 50 mV per division and the time scale is 10 μs (20 μs) for the left (right) plot.

about 40 μs the output voltage recovered. The results for smaller load changes are summarized in table 1. While the maximum voltage drop depends on the magnitude of the current change, the recovery time is nearly constant with values between 30 μs and 40 μs. The behaviour is different for load decreases and an example for the decrease from 6 A to 0 A is shown in figure 5. The maximum voltage overshoot was 320 mV and the recovery time for this setting was 90 μs. Table 1 contains the results for smaller current changes. In this case not only the maximum voltage overshoot but also the recovery time was dependent on the amplitude of the current decrease. While the amplitude of the voltage error was similar compared to the first measurement, the recovery time was larger.

Table 1. Maximum voltage under- and overshoot and recovery times for different load changes.

load change	peak voltage drop	recovery time
0 A -> 1 A	−60 mV	30 μs
0 A -> 2 A	−120 mV	30 μs
0 A -> 3 A	−175 mV	40 μs
0 A -> 4 A	−225 mV	40 μs
0 A -> 5 A	−275 mV	40 μs
0 A -> 6 A	−350 mV	40 μs
1 A -> 0 A	60 mV	50 μs
2 A -> 0 A	125 mV	55 μs
3 A -> 0 A	175 mV	60 μs
4 A -> 0 A	220 mV	70 μs
5 A -> 0 A	275 mV	80 μs
6 A -> 0 A	320 mV	90 μs

## 4.3 Emission spectrum measurements

In this subsection we present the measurements with the spectrum analyser (see figure 6). The background level with the selected settings was −120 dBm. We did not observe any emissions
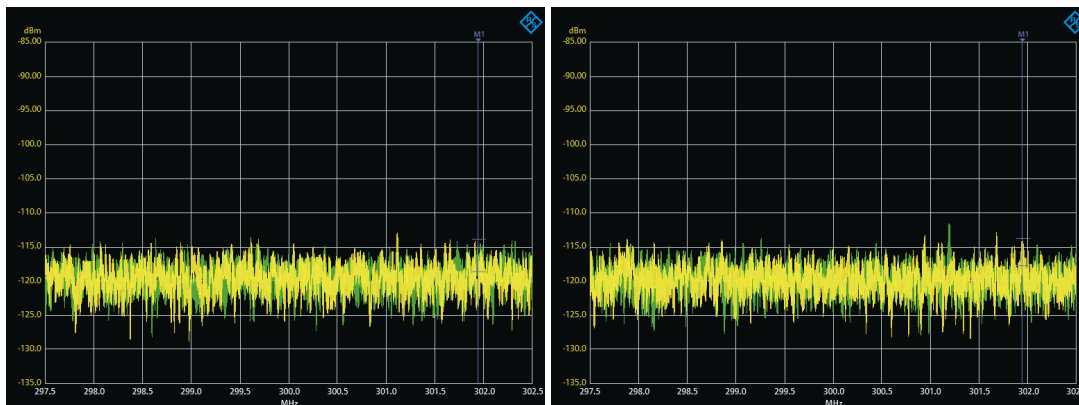
Figure 6. Measured emission spectra (green) compared to be background (yellow) on the top (left) and bottom (right) of the converter module, running at 4 A load and 16 V input voltage.

from our power converter between 297.5 MHz and 302.5 MHz. In addition no differences between emissions from the top and the bottom side of converter module were visible. Since we did not see radiated power in the near field at frequencies around 300 MHz, there will be also no power in the far field.

4.4 MRI measurements
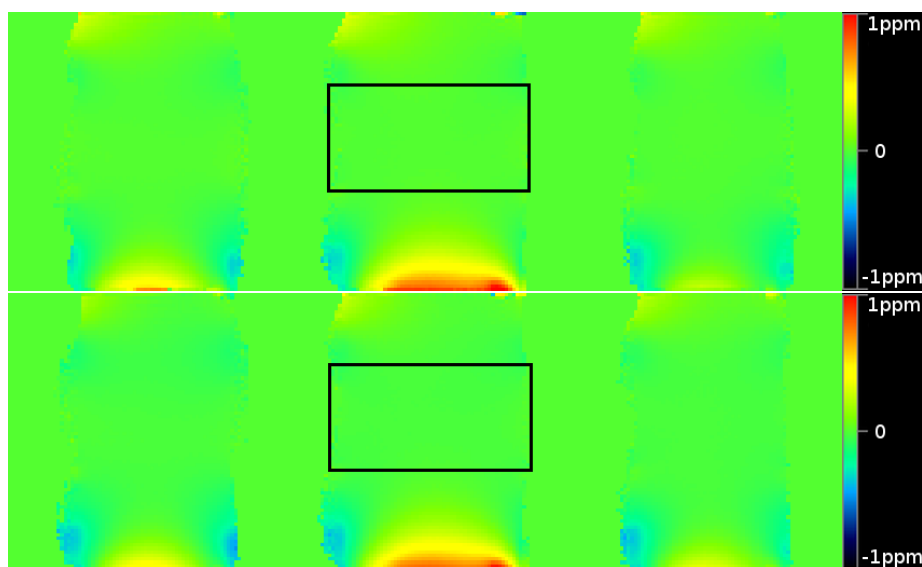
Figure 7. The measured MR B_0-map with running converter (top) compared to the baseline measurement (bottom). The black boxes indicate the shimming area.

The measured B_0-maps are shown in figure 7. The maximum deviations in the shimmed area were around 0.2 ppm and about 1 ppm at the edge of the field of view. The results from the SNR measurements are summarized in table 2. There was a slight decrease in the signal-to-noise ratio (about 2 %) after placing the converter module into the MRI, with attached cabling but without powering. The value remains constant while the converter is powered on with different loads.

Table 2. Normalized SNR ratio, obtained from the Bruker QA SNR sequence.

setup	normalized SNR
a) baseline (no converter)	$4127(48)\,\mathrm{mm}^{-3}$
b) converter in, powered off	$4038(29)\,\mathrm{mm}^{-3}$
c) powered on, 2 A load	$4050(20)\,\mathrm{mm}^{-3}$
d) powered on, 4 A load	$4048(55)\,\mathrm{mm}^{-3}$

5 Discussion

5.1 Static measurements

The expectation for the load measurement based on the datasheet of the controller ASIC is a very minor (1 mV) voltage drop from 0 A to 0.5 A and then again a small increase (up to 1 mV) from 3 A onwards. Due to the linear voltage drop with increasing output current we assume that our converter module (including the connectors) has a serial resistance of $12\,\mathrm{m\Omega}$. Even though the observed behaviour is different from the expectation, the absolute voltage drop is smaller than 75 mV. We will take this into account in the design of our electronics boards. The line regulation (total absolute deviation < 0.1 percent) is in accordance with the manufacturer's specification.

The measurements for efficiency in the datasheet are not given for our operation point (coil inductance: $2.2\,\mathrm{\mu H}$, switching frequency: 2 MHz, output voltage: 2.4 V), so that a direct comparison is not possible. We achieved values between 70 % and 87 %, which are more than sufficient for our application. Especially for the foreseen operation voltage of 16 V, the efficiency is above 80 % for output currents between 1.5 A and 5 A. The decrease in the efficiency for small output currents is caused by the constant idle input current of the converter module (about 40 mA). For low output powers and high input voltages, this particularly influences the overall efficiency.

We observed a slight decrease in conversion efficiency with increasing temperature. The measurements were taken in still air at about 25 °C ambient temperature. The device's temperature did not exceed the measured 75 °C at any moment. Therefore, we can operate the converter with continuous output currents of up to 4 A in a still air environment.

5.2 Dynamic measurements

The load transients caused voltage drops and overshoots of the order of 300 mV for a maximum load change of 6 A. For realistic load changes (3 A) the maximum deviation is 175 mV. We will bear this behaviour in mind for the design of our hardware. In our design, we use the DC-DC converters only for the supply of the intermediate rails, so that there are additional capacitors and LDOs, which can compensate for the observed voltage spikes. The maximum voltage drop is taken into account for the calculation of the voltage head room for the LDOs, such that their output voltage will always be as required.

5.3 Emission spectrum measurements

There was no visual difference between the background spectrum and the spectrum from the converter while operating. We conclude that the low-emission design, in combination with the copper shielding, suppresses the high-frequency electromagnetic emissions. This is one of the main requirements for operation inside the MRI.

5.4 MRI measurements

Inside the shimmed volume, the B_0 distortions are neglectable. Towards the edges of the field of view the deviation increases but remains still below 1 ppm, which is fine for all MRI measurements. The small decrease of the SNR value observed after the placement of the converter in the MRI indicates that we couple external noise into the machine. Since we could not observe any further degradation after powering the converter, we conclude that the converter itself does not disturb the MRI. This observation is in accordance with our measurement with the spectrum analyser.

5.5 Effects of the MRI's gradient system

The MRI uses magnetic pulses for spatial encoding, which have a frequency of about 1 kHz and that induce a current in every conductor loop. We did not observe any degradation in the performance of the DC-DC converter due to these pulses. The effect depends on the cross section A of a conductor loop and the slew rate of magnetic fields of the gradient system. The maximum slew rate is $s = 640\,\mathrm{T/sm}$ in each direction. The induced voltage U_ind in a conductor loop is given by the law of induction:

$$U_\mathrm{ind} = nA\frac{dB}{dT} = nAls = nwl^2s$$

with the number of windings n (for coils only), the length l in the direction of the field change and the width w perpendicular to that direction. The maximum induced voltage is below 15 mV, which is less than 1 % of the output voltage. Furthermore, the gradient pulses have a low frequency of about 1 kHz compared to the operation frequency of the converter ($> 2\,\mathrm{MHz}$). The controller ASIC can compensate the induced voltages such that the gradient pulses have no measurable influence on the performance of the power converter.

6 Conclusion & outlook

The goal of this work was the development of a compact MR-compatible DC-DC converter module. The device described has been tested successfully. We reached efficiencies above 80 % without disturbing the MRI during realistic operation conditions. The device fulfils all of our expectations and allows a significant simplification of the powering concept of our detector hardware. Based on this successful test, we will design the SAFIR insert to operate with only one 16 V input voltage.

References

[1] R. Becker et al., *Studies of the high rate coincidence timing response of the STiC and TOFPET ASICs for the SAFIR PET scanner*, 2016 *JINST* **11** P12001.

[2] R. Becker et al., *The SAFIR experiment: Concept, status and perspectives*, *Nucl. Instrum. Meth.* **A 651** (2017) 651.

[3] M. Ahnen et al., *Performance measurements of the SAFIR prototype detector with the STiC ASIC readout*, *IEEE Trans. Rad. Plasma. Med. Sci.* **2** (2018) 250.

[4] C. Tsoumpas, D. Visvikis and G. Loudos. *Innovations in small-animal PET/MR imaging instrumentation*, *PET Clinics* **11** (2015) 105.

[5] R. Becker et al., *Monte-Carlo simulation based estimation of NECR, sensitivity, and spatial resolution of a novel preclinical PET insert for MR*, in the proceedings of the *2015 IEEE Nuclear Science Symposium and Medical Imaging Conference (NSS/MIC)*, October 31–November 7, San Diega, U.S.A. (2015).

[6] L. Biagi et al., *Evaluation of DC/DC switching power regulation with small-scale integrated inductors for PET/MR*, *EJNMMI Phys.* **2** (2015) A14.

[7] ALTERA, *Enpirion power datasheet EN6347QI 4 A Power SoC voltage mode synchronous PWM buck with integrated inductor*, rev. 1 (2016).

[8] S. Dhawan et al., *Ideas on DC-DC converters for delivery of low voltage and high currents for the SLHC/ILC detector electronics in magnetic field and radiation environments*, in the proceeidngs of the 12th *Workshop on Electronics For LHC and Future Experiments*, September 25–29, Valencia, Spain (2007).

[9] CMS collabroation, *The CMS experiment at the CERN LHC*, 20018 *JINST* **3** S08004.

[10] CERN, *FEASTMP radiation and magnetic field tolerant 10 W DC/DC converter module*, rev. 2.1 (2014).

[11] Linear Technology, 42 *V,* 6 *A Synchronous Step-Down Silent Switcher 2 with 2.5 μA quiescent current*, Rev. A (2017).

[12] Texas Instruments, *AN-2155 layout tips for EMI reduction in DC/DC converters*, rev. 1 (2013).